

1 **Estimating a Size-Specific Dose for Helical Head CT Examinations Using Monte Carlo Simulation**
2 **Methods**

3
4 Anthony J. Hardy, MS^{1,2}; Maryam Bostani, Ph.D^{1,2}; Andrew M. Hernandez, Ph.D³; Maria Zankl, MSc⁴;
5 Cynthia McCollough, Ph.D⁵; Chris Cagnon, Ph.D^{1,2}; John M. Boone, Ph.D³; Michael McNitt-Gray,
6 Ph.D^{1,2}
7

8 ¹Department of Radiology, David Geffen School of Medicine, University of California, Los Angeles, Los
9 Angeles, California, 90024

10 ²Physics and Biology in Medicine Graduate Program, David Geffen School of Medicine, University of
11 California, Los Angeles, Los Angeles, California, 90024

12 ³Departments of Radiology and Biomedical Engineering, Biomedical Engineering Graduate Group,
13 University of California Davis, Sacramento, California 95817

14 ⁴Helmholtz Zentrum München, German Research Center for Environmental Health (GmbH), Institute of
15 Radiation Protection, Ingolstaedter Landstrasse 1, Neuherberg 85764, Germany

16 ⁵Department of Radiology, Mayo Clinic, Rochester, MN, 55905

17
18 ***Corresponding Author**
19 924 Westwood Blvd, Suite 650
20 Los Angeles, CA 90024, USA
21 Phone: (310) 481-7558
22 ahardy@mednet.ucla.edu

23

24

25

26

27

28

29 **Purpose**

30 Size Specific Dose Estimates (SSDE) conversion factors have been determined by AAPM Report 204 to
31 adjust $CTDI_{vol}$ to account for patient size but were limited to body CT exams. The purpose of this work
32 was to determine conversion factors that could be used for an SSDE for helical, head CT examinations for
33 patients of different sizes.

34

35 **Methods**

36 Validated Monte Carlo (MC) simulation methods were used to estimate dose to the center of the scan
37 volume from a routine, helical head exam for a group of patient models representing a range of ages and
38 sizes. Ten GSF/ICRP voxelized phantom models and five pediatric voxelized patient models created
39 from CT image data were used in this study. CT scans were simulated using a Siemens MDCT equivalent
40 source model. Scan parameters were taken from the AAPM Routine Head protocols for a fixed tube
41 current (FTC), helical protocol and scan lengths were adapted to the anatomy of each patient model. MC
42 simulations were performed using mesh tallies to produce voxelized dose distributions for the entire scan
43 volume of each model. Three tally regions were investigated: (1) a small 0.6 cc volume at the center of
44 the scan volume, (2) 0.8-1.0 cm axial slab at the center of the scan volume, and (3) the entire scan
45 volume. Mean dose to brain parenchyma for all three regions was calculated. Mean bone dose and a
46 mass-weighted average dose, consisting of brain parenchyma and bone, were also calculated for the slab
47 in the central plane and the entire scan volume. All dose measures were then normalized by $CTDI_{vol}$ for
48 the 16 cm phantom ($CTDI_{vol,16}$). Conversion factors were determined by calculating the relationship
49 between normalized doses and water equivalent diameter (D_w).

50

51 **Results**

52 CTDI_{vol,16}-normalized mean brain parenchyma dose values within the 0.6 cc volume, 0.8-1.0 cm central
53 axial slab, and the entire scan volume, when parameterized by D_w , had an exponential relationship with a
54 coefficient of determination of 0.86, 0.84, and 0.88, respectively. There was no statistically significant
55 difference between the conversion factors resulting from these three different tally regions. Exponential
56 relationships between CTDI_{vol,16}-normalized mean bone doses had coefficients of determination of 0.83
57 and 0.87 for the central slab and for the entire scan volume, respectively. CTDI_{vol,16}-normalized mass-
58 weighted average doses had coefficients of determination of 0.39 and 0.51 for the central slab and for the
59 entire scan volume, respectively.

60

61 **Conclusions**

62 Conversion factors that describe the exponential relationship between CTDI_{vol,16}-normalized mean brain
63 dose and a size metric (D_w) for helical head CT exams have been reported for two different interpretations
64 of the center of the scan volume. These dose descriptors have been extended to describe the dose to bone
65 in the center of the scan volume as well as a mass weighted average dose to brain and bone. These may
66 be used, when combined with other efforts, to develop an SSDE dose coefficients for routine, helical head
67 CT exams.

68

69 **Keywords: Size-specific dose estimate, Monte Carlo dose simulations, head CT**

70

71

72 **1. INTRODUCTION**

73 A recent study conducted by the University of California Dose Optimization and Standardization
74 Endeavor (UC Dose) summarizing CT doses across twelve University of California medical centers found
75 that head scans comprised 16% of all adult CT examinations.¹ The same study also found that the most
76 frequent area imaged in pediatric patients was the head, accounting for 33% of the total procedures
77 administered.¹ The fact that radiation exposure from head CT examinations is a large contributor to the
78 total medical radiation exposures underscores the need for accurate patient dose assessments from head
79 CT procedures, particularly for younger patients.

80 The radiation dose metric commonly reported on most scanners is the volume computed
81 tomography dose index ($CTDI_{vol}$).^{2, 3} This metric, however, is a measure of dose to a reference phantom,
82 not a measure of patient dose.^{2, 3} Turner et al. showed that utilizing $CTDI_{vol}$ as normalization metric for
83 Monte Carlo (MC) simulated organs doses from abdominal CT scans compensated both for the
84 differences among scanner manufacturers and reduced the variation of organ doses across scanners from
85 31.5% down to 5.2%.⁴ Subsequently, AAPM Report 204 developed the size-specific dose estimate
86 (SSDE) quantity to adjust $CTDI_{vol}$ using a set of $CTDI_{vol}$ -to-patient-dose conversion coefficients from
87 either the 32 cm CTDI reference phantom ($CTDI_{vol,32}$) or the 16 cm phantom ($CTDI_{vol,16}$) to account for
88 patient size in adult and pediatric body CT exams, respectively.⁵ SSDE "...provides an estimate of the
89 dose at the center of the scanned region (along z) in the patient" and is defined as the patient dose
90 estimates that takes into account corrections based on patient size by AAPM Report 204.⁵ Although
91 SSDE has been shown to be a good substitute for organ dose in the context of abdominal scans,⁶ the work
92 of AAPM Report 204 was limited only to body CT examinations.

93 The work of McMillan et al. in 2014 sought to extend the approach developed by Turner et al.
94 and used in AAPM Report 204 for the body, to investigate organs of interest in the head, including brain
95 and lens of eye, for routine helical and axial acquisitions.⁷ In that study, strong predictive exponential
96 correlations were observed when MC simulated organ doses from detailed voxelized phantom were
97 normalized by $CTDI_{vol,16}$ and were parameterized by water equivalent diameter (D_w) as a metric of patient

98 size,⁸ yielding coefficients of determination (R^2) of 0.93 for whole brain dose for helical scans.⁷ While
99 predictive correlations were determined by McMillan et al., that work focused on organ doses rather than
100 dose to the center of the scan volume, the latter being consistent with SSDE as defined in AAPM Report
101 204.⁵

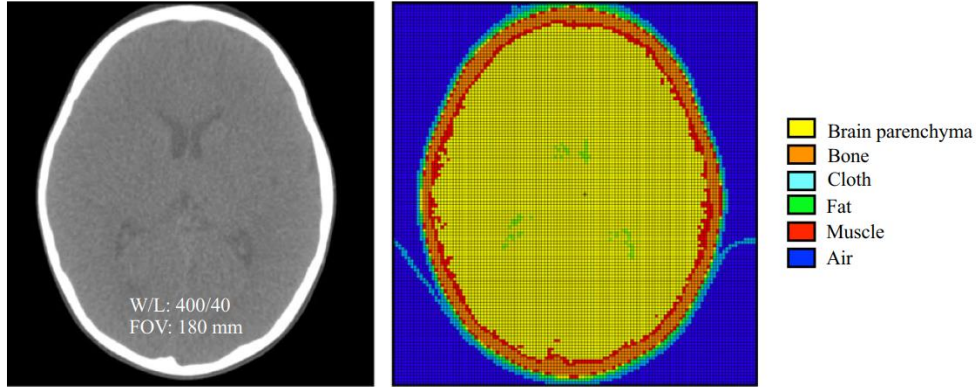
102 Therefore, the purpose of this current study was to estimate dose to the “center of the scan
103 volume” for helical head CT exams that can be used to help determine conversion factors for an SSDE of
104 the head. AAPM Report 204 described that the Size Specific Dose Estimate (SSDE) gives an estimate of
105 the dose at “the center of the scanned region (along z) in the patient.”⁵ However for helical head CT
106 exams, the definition of the “center of the scanned region (along z)” is open to several interpretations,
107 which are explored in this manuscript to determine if there was any difference in results based on these
108 interpretations. Therefore, this work employed voxelized patient models along with MC simulation
109 techniques with mesh tallies of the entire head to produce voxelized dose distributions wherein two
110 different interpretations of “center of the scan volume” were investigated: a small central region within
111 the brain parenchyma and a central slab comprising both brain parenchyma and bone of the cranium.
112 Additionally, the entire scan volume was also investigated for sake of comparison and completeness. In
113 the case of the central slab, as well for the entire scan volume, doses both to the brain parenchyma and
114 bone were also estimated separately. To account for the dose deposited in both the brain parenchyma and
115 bone in the head, a mass weighted-average dose comprising both brain parenchyma and bone was devised
116 to account for the presence of both brain parenchyma and bone within the slab tally region, as well as for
117 the entire scan volume. In a manner similar to that used in AAPM Report 204, all doses were normalized
118 by $CTDI_{vol,16}$ and were parameterized in an exponential fashion with D_w .

119 2. MATERIALS AND METHODS

120 2.A Patient models

121 Ten voxelized phantom models from the GSF (Gesellschaft für Strahlen- und Umweltforschung;
122 National Research Centre for Environment and Health – current name: Helmholtz Zentrum München,
123 German Research Center for Environmental Health, Institute of Radiation Protection, Neuherberg,
124 Germany) family⁹ and the ICRP (International Commission on Radiological Protection) voxelized
125 reference male and female^{10, 11} were used with all radiosensitive organs identified. The eight GSF voxel-
126 based models were created from CT images with up to 131 organs and anatomic structures segmented.
127 The two ICRP reference male and female voxelized models were each based off modifications of two
128 corresponding male and female GSF models of similar external dimensions. The GSF/ICRP voxelized
129 models used in this study had the in-plane resolution subsampled from the original to decrease
130 computation time.⁹⁻¹¹

131 Additionally, to extend this investigation into the pediatric size range, the adult models were
132 augmented with five voxelized patient models created from anonymized head CT volume data sets of
133 pediatric patients. These data sets were obtained from clinically indicated scans under IRB approval.
134 **Figure 1** contains an example of an axial slice of a 23-month-old pediatric head CT scan and the
135 corresponding voxelized representation utilized in the MC simulations. All scans were acquired on a
136 Siemens Sensation 64 multi-detector row CT (MDCT) and were performed in the supine position. To
137 create voxelized models of each patient's anatomy from the image data, voxels within each image series
138 were modeled as either fat, water, muscle, bone or air and were subdivided into one of seventeen density
139 levels depending on its CT number.¹² Individual organs were not segmented for these patient models, but
140 brain parenchyma tissue was semi-automatically contoured and explicitly identified. The MCNPX model
141 characteristics for all voxelized models used in this study are summarized in **Table I**. Detailed
142 descriptions of scan length determination and patient size metrics in terms of D_w can be found in Sec. 2.B
143 and Sec. 2.C, respectively.



144

145 **Figure 1:** (Left) Head CT image of a pediatric patient (Peds5) who underwent a routine CT head exam
 146 with window/level settings and reconstruction field of view (FOV). (Right) Monte Carlo representation of
 147 the patient produced using a CT number-based lookup table. The image on the right is color-coded for the
 148 material designations for each voxel.

149

150 **Table I:** MCNPX model resolution characteristics, scan lengths, and D_w for GSF/ICRP phantom models
 151 and five patient models used in this investigation

Name	Age	Gender	In-plane resolution	Image slices	Lateral width (mm)	Anterior-posterior width (mm)	Slice thickness (mm)	Scan length (cm)	D_w (cm)
Peds2*	7 d	Male	128 × 128	30	3.5	3.5	4.8	14.3	12.6
Peds1*	7 wk	Male	128 × 128	24	3.5	3.5	4.8	11.6	10.6
Baby	8 wk	Female	67 × 69	142	3.4	1.7	4.0	10.2	11.1
Peds3*	21 mo	Female	128 × 128	36	3.9	3.9	4.8	16.7	15.6
Peds5*	23 mo	Male	128 × 128	30	3.5	3.5	4.8	14.8	17.1
Peds4*	2 yr	Male	128 × 128	30	3.5	3.5	4.8	14.5	15.7
Child	7 yr	Female	64 × 64	144	6.2	6.2	8.0	14.8	17.2
Helga	28 yr	Female	64 × 64	114	7.8	7.8	10.0	14.5	18.2
Irene	32 yr	Female	66 × 66	348	7.5	3.8	5.0	15.8	17.1
Golem	38 yr	Male	64 × 64	220	8.3	8.3	8.0	15.6	18.3
Visible Human	38 yr	Male	64 × 64	250	8.6	4.3	5.0	15.3	19.6
Regina	38 yr	Female	75 × 69	348	7.1	3.6	4.8	17.1	19.9
Donna	40 yr	Female	64 × 64	179	7.5	7.5	10.0	16.5	18.7
Rex	43 yr	Male	64 × 64	222	8.6	4.3	8.0	16.0	20.2
Frank	48 yr	Male	64 × 64	193	5.9	5.9	5.0	21.8	19.2

152 * Indicates a voxelized patient model created from image data obtained from clinically indicated scans

153

154

155

156 **2.B. CT scanner and scanning protocol**

157 The scanning protocol used in this investigation was taken from the AAPM Adult Routine Head
158 CT protocol for a Siemens Sensation 64 MDCT.¹³ **Table II** contains the CT scanning protocol used in this
159 investigation. All simulations were performed as fixed tube current (FTC) helical scans with the
160 voxelized models centered within the gantry and with the patient table removed. The scan range was
161 defined from the top of the C1 lamina through the top of the calvarium.¹³ The widest nominal collimation
162 setting of 28.8 mm (measured beam width of 32.2 mm) on the Siemens scanner was used in the
163 simulations because it is the most dose efficient collimation setting.⁷ The AAPM’s Routine Head CT
164 protocol recommends either the gantry or head be tilted to reduce the dose to the lens of the eye;¹³
165 however, for the scanner being modeled, helical scans are not performed with gantry tilt, so no tilt angle
166 was used in these simulations.

167 **Table II:** Routine helical head FTC scanning protocol and associated CTDI_{vol,16}/mAs for the scanner used
168 in this investigation

Parameter	Setting
kV	120
Rotation time (s)	0.5
Helical pitch	0.55
Nominal collimation (mm)	28.8
Bowtie filter	Standard
Central Half Value Layer	8.9 mm Al
CTDI _{vol,16} /mAs (mGy/mAs)	0.24

169

170

171 **2.C Size Metrics**

172 D_w is a size metric referenced in AAPM Report 220 as the “x-ray attenuation of a patient in terms
173 of a water cylinder having the same x-ray absorption” and was used in this study as a measure of patient
174 size.⁸ For the five pediatric patients, D_w was estimated at the center of the scan volume directly from the
175 CT numbers (in Hounsfield units, HU) in their image data. For the GSF/ICRP models, it is not possible to
176 directly calculate D_w since they are constructed with pixel data containing tissue identification numbers,

177 not CT numbers. The D_w estimates for GSF/ICRP voxelized phantoms were instead obtained indirectly
178 from a correlation between effective diameter and D_w .⁷

179

180 **2.D Monte Carlo simulations**

181 All CT dose simulations for this investigation were conducted using a modified version of the
182 radiation transport software package MCNPX (Monte Carlo N-Particle eXtended version 2.7.a).¹⁴⁻¹⁶
183 Specifically, the source code was modified to model a MDCT scanner geometry and X-ray source
184 trajectory. All simulations were conducted in photon transport mode with a 1 keV low-energy cut-off.
185 This transport mode does not transport secondary electrons and instead assumes their energy to be
186 deposited at the interaction site. All MC CT dosimetry for helical head scans were performed using an
187 equivalent source model of the Siemens Sensation 64 MDCT scanner.¹⁷ The equivalent source model, as
188 previously described by Turner et al., generates and incorporates scanner-specific x-ray spectra and
189 bowtie filter profiles.¹⁷

190 Concerning the voxelized models mentioned in Sec. 2.A, incorporation into MCNPX simulations
191 required that each model be represented as a three-dimensional matrix of organ or non-anatomic material.
192 Integer identification numbers were allocated for material descriptions based on elemental compositions
193 of tissue substitutes and their densities as defined in ICRU Report 44.^{10,12,19} Three-dimensional dose
194 distributions of the entire head of each voxelized model were produced using the track-averaged
195 rectangular mesh tally configuration (RMESH) in MCNPX. This tally configuration tracks particles
196 through a mesh grid that is independent of the regular transport problem.¹⁴ The mesh tally grid was
197 defined to match the matrix size and resolution of each individual voxelized model to ensure that the dose
198 on a per voxel basis was accurately estimated. The average energy deposition within each voxel was
199 tallied in units of MeV/cm³/source particle.¹⁴ The resulting voxel-wise energy deposition maps were then
200 divided by a density map to get units of MeV/g/source particle.

201 Normalization factors are necessary to convert dose per simulated source particle (mGy/source
202 particle) to absolute dose per tube current time product (mGy/mAs). To achieve this, all MCNPX tally
203 results were multiplied by a scanner, collimation, and beam energy specific normalization factor.¹⁹ Each
204 simulation was performed with 10^8 photons to ensure a statistical uncertainty of less than 2% for each
205 individual mesh element. Because a mesh tally was used to investigate the dose distribution, the
206 computation time was on the order of 10-15 hours per voxelized model, depending on the resolution of
207 the phantom.

208

209 **2.E CTDI_{vol} measurements**

210 Since CT head scans performed in this study were all simulated scans, estimates of CTDI_{vol} were
211 needed for normalization purposes. Conventional CTDI₁₀₀ exposure measurements were taken at the
212 center and peripheral position of a CTDI_{vol,16} phantom with the scan parameters outlined in Sec 2.B.
213 Exposure measurements in milliroentgen (mR) were made with a standard 100 mm pencil ionization
214 chamber (Radcal, Monrovia, CA) coupled with a calibrated electrometer (MDH 1015, Radcal, Monrovia,
215 CA) and converted to units of air kerma (mGy) using the conversion factor $1 \text{ mR} = 0.00876 \text{ mGy}$. The air
216 kerma was then normalized by the tube current-rotation time product (mAs) used to take the initial
217 measurements. CTDI_{vol} was then calculated from the CTDI₁₀₀ measurements at the central and peripheral
218 locations and was recorded on an air kerma per tube current-rotation time product basis (mGy/mAs).

219

220

221 **2.F Dose analyses**

222 All dose values for each voxel in the patient models were obtained using mesh tallies as outlined
223 in Sec 2.D. Three regions were investigated in this study: (1) a small 0.6 cc volume at the center of the
224 scan volume, (2) a 0.8-1.0 cm axial slab at the center of the scan volume, and (3) the entire scan volume.
225 A representation of each tally region is shown in **Figure 2**. Tally regions #1 and #2 were investigated as

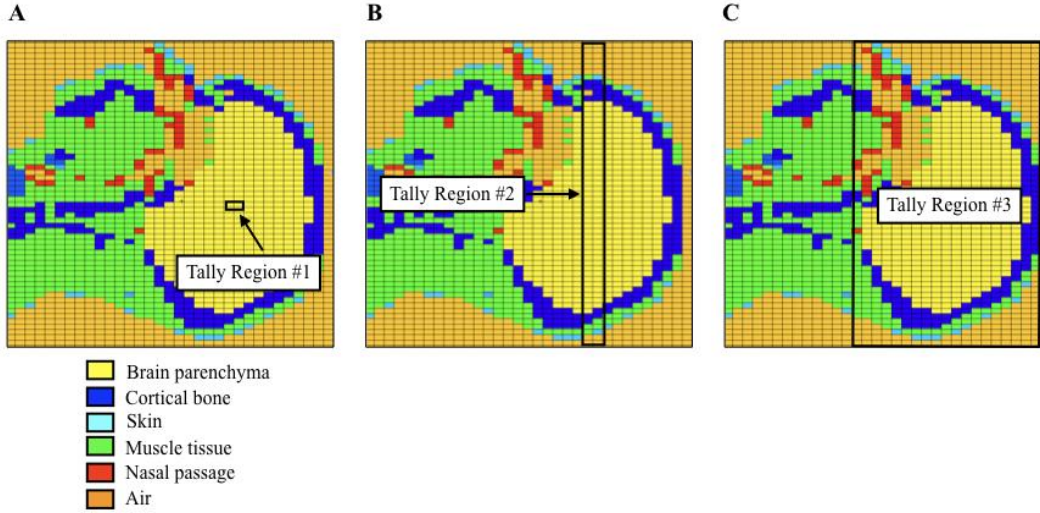
226 separate interpretations of “center of the volume.” For tally region #1, a 0.6 cc volume was positioned at
 227 the center of the scan volume and the mean brain parenchyma dose values within all voxels in this small
 228 volume were averaged. Tally #1 was used to simulate within MCNPX a dose reading from the irradiation
 229 of a Farmer chamber virtually located in the center of head. The coefficient of variations (CV; ratio of
 230 standard deviation to the mean) were also recorded. This configuration was used to mimic a dose reading
 231 from the irradiation of 0.6 cc ion chamber virtually located in the center of head.

232 For tally region #2, dose values within a slab parallel to an axial plane at the center of the scan
 233 volume were identified. The thickness of the slab ranged from 0.8 – 1.0 cm, depending on the slice
 234 thickness of the voxelized phantom, as detailed in **Table I** in Sec 2.A. Dose estimations within this slab
 235 consist of dose to the brain parenchyma and the bone surrounding it. Under this configuration, the mean
 236 of the dose voxels to both brain parenchyma and bone within the slab were calculated. The standard
 237 deviation and coefficient of variation for both brain parenchyma and bone dose within the slab were also
 238 calculated. Additionally, to consider the presence of both brain parenchyma and bone in tally #2 and tally
 239 #3, a mass-weighted average of dose contributions from both brain tissue and bone was calculated using

240 **Equation 1,**

$$241 \quad D_{wt-avg} = \frac{D_{bone}M_{bone} + D_{brain}M_{brain}}{M_{bone} + M_{brain}} \quad (1)$$

242 where D_{bone} and D_{brain} are the mean dose contributions from bone and brain parenchyma, respectively, and
 243 M_{bone} and M_{brain} represent the mass contributions from bone and brain parenchyma, respectively.
 244 Similarly, the mean of the dose voxels of both brain parenchyma and bone within the entire scan volume
 245 were calculated, as well as a mean mass-weighted average dose. The standard deviations and coefficients
 246 of variation for brain parenchyma and bone doses within the entire scan volume were also recorded. In
 247 this study, mean doses are designated using the nomenclature $D_{tissue,tally\ region}$ where *tissue* represents the
 248 tissue type and *tally region* represents one of the three tally regions. The tissue contents and doses
 249 calculated within each tally region are summarized in **Table III**.



250

251 **Figure 2:** MCNPX voxelized representation of ICRP male “Rex” depicting **A)** the 0.6 cc volume
 252 positioned at the center of scan volume (tally region #1), **B)** the 0.8-1.0 cm axial slab positioned at the
 253 center of the scan volume (tally region #2), and **C)** the entire scan volume (tally region #3) as specified by
 254 the AAPM Routine Head CT¹³ protocols with corresponding color-coded material designation for each
 255 voxel.

256
257

258 **Table III:** Summary of tally regions, tissue contents within each tally region, and mean dose estimates
 259 measured

Tally region	Tissue(s) in tally region	Doses calculated
#1: 0.6 cc volume	Brain parenchyma	$D_{\text{brain},1}$
#2: Central slab	Brain parenchyma, bone	$D_{\text{brain},2}, D_{\text{bone},2}, D_{\text{wt-avg},2}$
#3: Entire scan volume	Brain parenchyma, bone	$D_{\text{brain},3}, D_{\text{bone},3}, D_{\text{wt-avg},3}$

260

261 All dose values were normalized by $\text{CTDI}_{\text{vol},16}$. Consistent with AAPM Report 204, normalized
 262 dose values were parameterized as a function D_w using the following exponential relationship:

$$263 \frac{D_{\text{tally region, tissue}}}{\text{CTDI}_{\text{vol}}} = A \times e^{-B \times D_w} \quad (2)$$

264 where A and B (units of cm^{-1}) are regression constants for a given tissue classification. The coefficient of
 265 determination (R^2) was used to assess the ability of the correlations to explain the proportion of variation
 266 explained by D_w .

267 Dose matrix analysis was performed using MATLAB scripts (R2014b, TheMathWorks, Inc.,
 268 Natick, Massachusetts, United States). Brain parenchyma dose voxels from all three tally regions were

269 compared using the one-way analysis of variance (ANOVA). ANOVA was also performed to compare
270 conversion factors from AAPM Report 204 for a $CTDI_{vol,16}$ phantom with normalized brain parenchyma
271 dose voxels from the three tally regions. Bone doses for tally regions #2 and #3 were compared using a
272 paired t-test. Additionally, percentage difference between $D_{bone,2}$ and $D_{bone,3}$ was tabulated. Similarly,
273 mass-weighted average doses for tally regions #2 and #3 were also compared using a paired t-test and
274 percentage difference between $D_{wt-avg,2}$ and $D_{wt-avg,3}$ was tabulated. ANOVA was also performed to
275 compare conversion factors from AAPM Report 204 with mass-weighted average doses from tally
276 regions #2 and #3. Statistical analyses were performed using GraphPad Prism 6.00 for Mac OS X
277 (GraphPad Software, La Jolla, California, USA, www.graphpad.com).

278

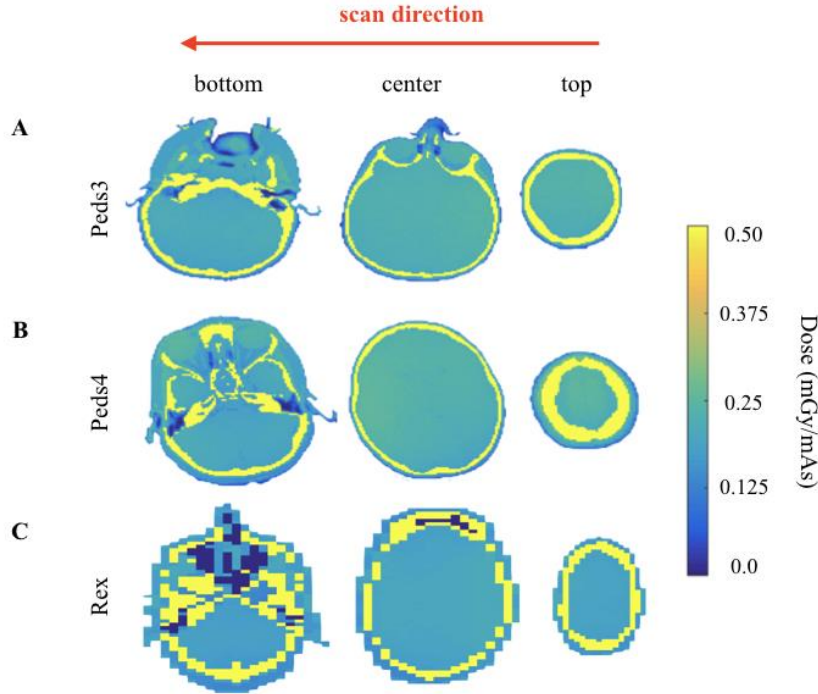
279

280 **3. RESULTS**

281 **3.A. Mesh tally results**

282 Dose distribution maps from the mesh tally simulations of three different voxelized models are
283 shown in **Figure 3**. These mesh tally results provide a graphical representation of the uniformity of the
284 dose distribution within the brain parenchyma. Each of the following sections below describes the doses
285 for each tissue group: brain parenchyma dose, bone dose, and the mass-weighted average of brain
286 parenchyma and bone dose.

287



288

289 **Figure 3:** Axial view of voxelized dose distribution maps for Peds3 (A), Peds4 (B), and Rex (C),
 290 respectively, at the top, center, and bottom of the scan volume. The red arrow at the top of the figure
 291 indicates the direction of the scan range.

292

293 3.A.1 Brain parenchyma doses

294 $D_{\text{brain},1}$, $D_{\text{brain},2}$, and $D_{\text{brain},3}$, for each voxelized model can be seen in **Table IV** with values ranging
 295 from 0.188 mGy/mAs to 0.292 mGy/mAs, 0.185 mGy/mAs to 0.286 mGy/mAs, and 0.178 mGy/mAs to
 296 0.284 mGy/mAs, respectively. This table also shows that the CV were below 2.6%, 6.5%, and 9.4%
 297 within tally regions #1, #2, and #3, respectively, across all voxelized models and below 3.9% across all
 298 tally regions *within* each voxelized model. ANOVA analysis with multiple comparison showed that
 299 $D_{\text{brain},1}$, $D_{\text{brain},2}$, and $D_{\text{brain},3}$ were not significantly different from each other [$F(2, 42) = 0.07, p = 0.93$].

300

301

302 **Table IV:** Mean brain doses by tally region type with coefficients of variation within each tally region,
 303 and the coefficient of variation across tally regions for each patient

<u>0.6 cc volume (#1)</u>	<u>Slab (#2)</u>	<u>Entire scan volume (#3)</u>	<u>Across</u>
---------------------------	------------------	--------------------------------	---------------

Name	$D_{\text{brain},1}$		$D_{\text{brain},2}$		$D_{\text{brain},3}$		Regions
	(mGy/mAs)	CV	(mGy/mAs)	CV	(mGy/mAs)	CV	CV
Peds2	0.257	2.6%	0.254	4.2%	0.273	5.0%	3.9%
Peds1	0.290	1.7%	0.286	5.3%	0.284	4.8%	1.1%
Baby	0.292	1.4%	0.286	3.4%	0.283	5.6%	1.6%
Peds3	0.230	2.5%	0.226	4.0%	0.238	7.3%	2.6%
Peds5	0.200	2.6%	0.197	4.8%	0.197	5.9%	0.9%
Peds4	0.217	2.0%	0.215	4.8%	0.216	6.7%	0.5%
Child	0.229	1.9%	0.227	2.9%	0.221	4.9%	1.8%
Helga	0.204	1.3%	0.207	4.8%	0.198	7.1%	2.3%
Irene	0.212	1.2%	0.210	5.6%	0.204	6.4%	2.0%
Golem	0.217	0.8%	0.211	5.0%	0.208	5.9%	2.2%
Visible Human	0.188	1.7%	0.187	6.5%	0.180	9.4%	2.4%
Regina	0.216	2.5%	0.215	5.3%	0.207	7.8%	2.3%
Donna	0.210	2.8%	0.214	4.4%	0.203	7.1%	2.7%
Rex	0.197	0.8%	0.195	3.9%	0.189	5.9%	2.1%
Frank	0.190	1.4%	0.185	5.0%	0.178	9.2%	3.3%

304

305 3.A.2 Bone doses

306 $D_{\text{bone},2}$ and $D_{\text{bone},3}$ for each voxelized model ranged from 0.664 mGy/mAs to 1.040 mGy/mAs and
307 0.604 mGy/mAs to 0.957 mGy/mAs, respectively, as indicated in **Table V**. The coefficient of variation
308 for $D_{\text{bone},2}$ and $D_{\text{bone},3}$ was less than 27% and 29%, respectively, within the individual patient models and
309 differences of less than 12% were observed *across* all models. The differences between $D_{\text{bone},2}$ and $D_{\text{bone},3}$
310 were found to be statistically significant ($p < 0.0001$, using paired t -test).

311

312

313

314

315

316 **Table V:** Mean bone doses by tally region type with coefficients of variation within each tally region and
317 percentage differences between the means of each region
318

Name	Slab (#2)		Entire scan volume (#3)		Percentage Difference (%)
	D _{bone,2} (mGy/mAs)	CV	D _{bone,3} (mGy/mAs)	CV	
Peds2	0.929	8%	0.916	11%	1.4%
Peds1	0.917	27%	0.894	29%	2.5%
Baby	1.040	6%	0.957	14%	8.3%
Peds3	0.839	16%	0.768	21%	8.8%
Peds5	0.857	14%	0.768	19%	10.9%
Peds4	0.759	18%	0.731	24%	3.8%
Child	0.792	5%	0.733	15%	7.8%
Helga	0.734	10%	0.651	16%	12.0%
Irene	0.730	9%	0.697	12%	4.7%
Golem	0.723	8%	0.688	15%	11.0%
Visible Human	0.673	13%	0.603	18%	5.3%
Regina	0.730	9%	0.693	11%	5.0%
Donna	0.750	9%	0.680	13%	9.7%
Rex	0.661	8%	0.636	11%	3.9%
Frank	0.664	10%	0.604	17%	9.4%

319

320 3.A.3 Mass-weighted average

321 D_{wt-avg,2} and D_{wt-avg,3} ranged from 0.306 mGy/mAs to 0.397 mGy/mAs and 0.380 mGy/mAs to
322 0.472 mGy/mAs, respectively, across all voxelized models as indicated in **Table VI**. Differences of less
323 than 27% were observed between D_{wt-avg,2} and D_{wt-avg,3} for each of the individual patient models. In
324 addition, D_{wt-avg,3} was consistently higher than D_{wt-avg,2} across all patient models. These differences were
325 statistically significant ($p < 0.0001$, using paired t -test).

326

327

328

329

330

331

332

333

334
335

Table VI: The mass-weighted average of brain and bone dose for tally regions #2 and #3 ($D_{wt-avg,2}$, $D_{wt-avg,3}$) and the percentage differences between the means of each region.

Name	Slab (#2)	Entire scan volume (#3)	Percentage Difference (%)
	$D_{wt-avg,2}$ (mGy/mAs)	$D_{wt-avg,3}$ (mGy/mAs)	
Peds2	0.338	0.412	-20%
Peds1	0.366	0.436	-18%
Baby	0.397	0.472	-17%
Peds3	0.359	0.399	-11%
Peds5	0.326	0.408	-22%
Peds4	0.326	0.395	-19%
Child	0.324	0.397	-20%
Helga	0.311	0.398	-25%
Irene	0.328	0.417	-24%
Golem	0.351	0.411	-16%
Visible Human	0.332	0.380	-13%
Regina	0.306	0.402	-27%
Donna	0.350	0.427	-20%
Rex	0.317	0.379	-18%
Frank	0.361	0.401	-11%

336

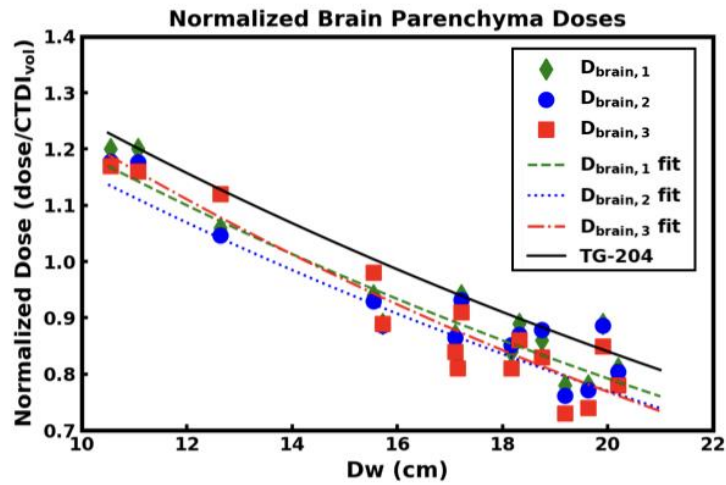
337

338 3.B Size-specific, scanner-independent dose estimates

339 3.B.1 Normalized brain parenchyma doses estimates and comparison with AAPM Report 204 values

340 **Figure 4** shows normalized brain parenchyma dose estimates for the three tally regions ($D_{brain,1}$,
341 $D_{brain,2}$, and $D_{brain,3}$) parameterized as functions of D_w . For comparison, AAPM Report 204 conversion
342 coefficients for the 16 cm pediatric body phantom as a function of D_w (Figure 6 from that report) are
343 included in the same figure. The coefficients of determination for normalized $D_{brain,1}$, $D_{brain,2}$, and $D_{brain,3}$
344 dose estimations were 0.86, 0.84, and 0.88, respectively. Results from the regression analysis are
345 summarized in **Table VII**. ANOVA showed there was no statistically significant difference between
346 $D_{brain,1}$, $D_{brain,2}$, $D_{brain,3}$ compared to the AAPM Report 204 conversion factors based on $CTDI_{vol,16}$ [$F(3, 56)$
347 $= 0.70$, $p = 0.56$]. However, it should be noted that estimates using AAPM report 204 conversion factors

348 were consistently higher by 5-10% than those obtained using the regression equations for $D_{\text{brain},1}$, $D_{\text{brain},2}$,
 349 and $D_{\text{brain},3}$ from **Table VII**.



350

351 **Figure 4:** Brain parenchyma dose estimations for the three tally regions ($D_{\text{brain},1}$, $D_{\text{brain},2}$, and $D_{\text{brain},3}$)
 352 normalized by $\text{CTDI}_{\text{vol},16}$ are plotted as a function of D_w along with the associated regression fits. AAPM
 353 Report 204 conversion factors based on $\text{CTDI}_{\text{vol},16}$ are also plotted for comparison.

354

355

356 **Table VII:** Regression analysis results for $D_{\text{brain},1}$, $D_{\text{brain},2}$, and $D_{\text{brain},3}$, along with AAPM Report 204
 357 regression curve coefficients

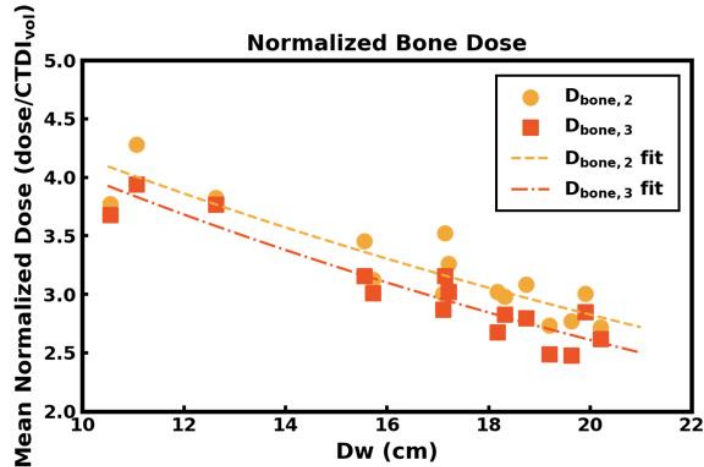
Normalized dose	A	B (cm^{-1})	R^2
$D_{\text{brain},1}$	1.80	0.041	0.86
$D_{\text{brain},2}$	1.74	0.041	0.84
$D_{\text{brain},3}$	1.93	0.046	0.88
AAPM Report 204	1.87	0.039	-

358

359 3.B.2 Normalized bone doses estimates

360 **Figure 5** contains normalized $D_{\text{bone},2}$ and $D_{\text{bone},3}$ parameterized as functions of D_w . The
 361 coefficients of determination for normalized $D_{\text{bone},2}$ and $D_{\text{bone},3}$ were 0.83 and 0.87, respectively. Results of
 362 the regression analysis are tabulated in **Table VIII**.

363



364

365

Figure 5: Normalized $D_{\text{bone},2}$ and $D_{\text{bone},3}$ with associated regression fits.

366

367

Table VIII: Regression analysis for normalized $D_{\text{bone},2}$ and $D_{\text{bone},3}$

Normalized Dose	A	B (cm^{-1})	R^2
$D_{\text{bone},2}$	6.17	0.039	0.83
$D_{\text{bone},3}$	6.17	0.043	0.88

368

369

370

371

372

373

3.B.3 Normalized mass-weighted average doses and comparisons to AAPM Report 204 values

374

375

Figure 6 shows normalized $D_{\text{wt-avg},2}$ and $D_{\text{wt-avg},3}$ parameterized as functions of D_w . The

376

coefficients of determination for normalized $D_{\text{wt-avg},2}$ and $D_{\text{wt-avg},3}$ were 0.39 and 0.51, respectively.

377

ANOVA revealed a statistically significant difference between AAPM Report 204 conversion factors and

378

normalized $D_{\text{wt-avg},2}$ and $D_{\text{wt-avg},3}$ dose estimations [$F(2,42) = 168.1, p < 0.0001$]. Results from the

379

regression analysis are summarized in **Table IX**. It should be noted here that the AAPM Report 204

380

values are consistently lower than the $D_{\text{wt-avg},2}$ and $D_{\text{wt-avg},3}$ dose estimations as indicated in Figure 6. The

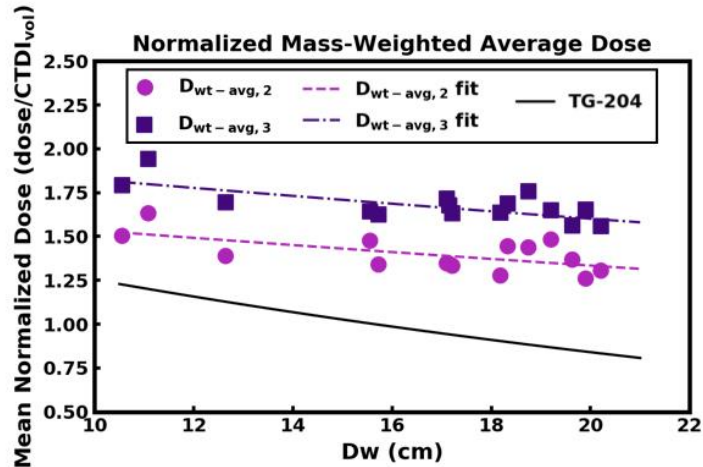
381

fit coefficients for AAPM Report 204 are the same as those in **Table VII**.

382

383

384



385

386 **Figure 6:** Normalized mass-weighted average dose to the brain parenchyma and cortical bone for tally
 387 regions #2 and #3 ($D_{wt-avg,2}$ and $D_{wt-avg,3}$) along with the associated regression fits. AAPM Report 204
 388 conversion factors based on $CTDI_{vol,16}$ are also plotted for comparison.

389

390

391

392

Table IX: Regression analysis for normalized $D_{wt-avg,2}$ and $D_{wt-avg,3}$

Normalized Dose	A	B (cm^{-1})	R^2
$D_{wt-avg,2}$	1.76	0.014	0.39
$D_{wt-avg,3}$	2.08	0.013	0.51

393

394

395 4. DISCUSSION AND CONCLUSIONS

396 In this study, Monte Carlo simulation methods were performed to obtain estimates of brain

397 parenchyma and bone dose from patients of different sizes and different tally configurations that could be

398 used as a basis for determining SSDE conversion coefficients for routine, helical head CT examinations.

399 Two different tally configurations were considered as possible candidates for the condition that the

400 measured dose be in the “center scan volume” as described in AAPM Report 204.⁵ In addition, a third

401 tally configuration estimates the dose to the entire scan volume of each patient for comparison. A mass-

402 weighted average dose quantity was used to consider the presence of bone in the central slab tally

403 configuration, as well for the entirety of the scan volume. Lastly, normalized brain parenchyma dose

404 estimations under all the three tally configurations and normalized mass-weighted average dose quantity
405 for the both slab and the entire scan volume were compared with conversion coefficients from AAPM
406 Report 204 based on $CTDI_{vol,16}$.

407 Normalized $D_{brain,1}$, $D_{brain,2}$, and $D_{brain,3}$ had R^2 of 0.86, 0.84 and 0.88, respectively. This indicates
408 that D_w provides good correlative function for the normalized brain parenchyma dose using the three tally
409 configurations investigated in this study. Unlike the study conducted by McMillan et al., which only
410 investigated normalized organ doses,⁷ the current study employed meshed tallies to map dose
411 distributions on a per voxel basis. Using this approach, $D_{brain,1}$, $D_{brain,2}$, and $D_{brain,3}$ were found to be
412 homogeneous with CVs below 10% across all voxelized models and below 4% across all tally regions
413 within each voxelized model. The implications of this result are twofold. The first is that if “center of the
414 scan volume” is defined as a small, central volume ($D_{brain,1}$) or a central slab within the brain parenchyma
415 ($D_{brain,2}$), then normalized doses within these regions should yield similar results for a head SSDE. The
416 second is that since the dose to the brain is fairly uniform, a dose measure from either of these two tally
417 regions would be similar to dose to the entire brain ($D_{brain,3}$).

418 $D_{bone,2}$ and $D_{bone,3}$ dose estimations had CVs as high as 29% and 27%, respectively. Variations of
419 surface dose as high as 30% for helical scans were previously observed by Zhang *et al.* as a consequence
420 of wider beam collimations and tube start angle.²⁰ When investigating the surface dose profile of a
421 $CTDI_{vol,32}$ phantom using MC, for example, Zhang *et al.* reported substantial dose peaks when utilizing a
422 pitch of less than one and when the simulated beam width was wider than the nominal beam width.²⁰ A
423 similar effect was seen when investigating the variability of surface dose in anthropomorphic phantoms in
424 the abdominal and thoracic regions, whereby a pitch of 0.75 was shown to result in a 37% increase in
425 surface dose.²⁰ The results of this study indicate that the dose variations observed within voxels of the
426 bone could be due to surface dose variations, particularly given the use of the low pitch and wide beam
427 collimations recommended in the AAPM’s Adult Routine Head CT Protocol.¹³

428 The coefficients of determination for normalized $D_{bone,2}$ and $D_{bone,3}$ were 0.83 and 0.87,
429 respectively, indicating that D_w is a satisfactory size metric for parameterization of normalized bone dose

430 either for a central slab (i.e., tally region #2) or for entirety of the head (i.e. tally region #3). The
431 motivation for investigating dose to bone as a function of patient size comes from the fact that, within the
432 cranium of pediatric patients, there is a fair amount of red bone marrow (RBM). The amount of RBM in
433 the head (relative to the entire body) is 12% for children 10 years of age and up to 29% for infants.^{21, 22}
434 The cranium is composed of the inner and outer layers of cortical bone that enclose bone spongiosa,
435 wherein RBM, yellow bone marrow (YBM), and trabecular bone are found.²² RBM is the primary tissue
436 of interest for the radiogenic risk of leukemia and is considered highly radiosensitive, as reflected by the
437 high tissue weighting designation in ICRP 103 ($w_T = 0.12$).²³ In this study, RBM and YBM were not
438 modeled. The cranial microdosimetry necessary to accurately assess RBM dose is beyond the scope of
439 this study, as is assessing the leukemia risk associated with head CT procedures. SSDE was only intended
440 to estimate patient dose using metrics of radiation output displayed by scanners and was not intended to
441 assess cancer risk from CT procedures.⁵ In routine head CT exams, although the cortical bone would
442 provide some shielding for the spongiosa containing RBM, RBM within the cranium would still receive
443 some appreciable amount of radiation dose. The potential effects of RBM dose should be taken into
444 consideration as a consequence of the scanning techniques used in routine head CT exams, particularly
445 for pediatric patients.^{23, 24}

446 In accordance with the second interpretation of “center of scan volume,” this study also
447 investigated dose to a central slab of the head, which consists of both bone and brain parenchyma. A mass
448 weighted-average of the dose contributions from both bone and brain parenchyma was devised to take
449 into consideration the presence of both tissue types. The coefficients of determination for normalized D_{wt-}
450 $_{avg,2}$ and $D_{wt-avg,3}$ were 0.39 and 0.51, respectively. The loss of an exponential relationship effects with
451 respect to the normalized mass-weighted average dose as a function of patient size can be explained by
452 considering the relationship between bone mass (and tissue mass) fraction of the head as a function of
453 patient size. The mass of bone increases with age which competes with the decreasing exponential of
454 normalized dose versus patient size. Weighting normalized doses of brain parenchyma and bone by their
455 respective masses accounts for the effects of size of the patients in effect, making the relationship of

456 normalized weighted average dose more linear with respect to patient size. Additionally, the statistically
457 significant difference observed between normalized $D_{wt-avg,2}$ and $D_{wt-avg,3}$ and AAPM Report 204 can be
458 attributed to the fact that, as mentioned in Sec 3.B.3, the conversion coefficients in AAPM Report 204
459 were devised for the abdomen region, which contains a small amount of bone relative to the percentage of
460 soft tissue. The values reported in AAPM Report 204 were consistently lower than normalized $D_{wt-avg,2}$
461 and $D_{wt-avg,3}$ due to taking the dose contributions of bone into consideration.

462 In several places in this manuscript, dose estimates were compared with AAPM Report 204
463 coefficients of SSDE to assess the generalizability of those coefficients to helical head scans when
464 estimating dose to the center of the scan volume. When estimating brain dose, **Figure 4** and **Table VII**
465 showed the $D_{brain,1}$, $D_{brain,2}$, and $D_{brain,3}$ estimates and the regression fits for each of these estimates, as well
466 as the SSDE-based estimates and coefficients. A one-way ANOVA showed no statistically significant
467 difference between the estimates obtained from the regression fits and those obtained using AAPM
468 Report 204 conversion factors; however, the SSDE-based estimates were consistently higher than those
469 provided by the regression fits of $D_{brain,1}$, $D_{brain,2}$, and $D_{brain,3}$. The differences observed between AAPM
470 Report 204 and normalized $D_{brain,1}$, $D_{brain,2}$, and $D_{brain,3}$ can be attributed to the fact that the AAPM Report
471 204 conversion factors were originally devised to estimate dose to the center of the scan volume for the
472 abdomen, which is a homogenous region comprised of soft tissue. The head, in contrast, is comprised of
473 the soft-tissue brain parenchyma encased in a layer of bone. The presence of the bone provides an
474 inherent source of shielding for the brain parenchyma, which decreases the normalized dose of the brain
475 parenchyma relative to the normalized dose to the center of the scan volume for the abdomen.

476 When estimating the mass-weighted average dose to brain parenchyma and cortical bone, **Figure**
477 **6** and **Table IX** showed the $D_{wt-avg,2}$ and $D_{wt-avg,3}$ estimates and the regression fits for each of these
478 estimates, as well as the SSDE-based estimates. This time, the one-way ANOVA analysis did show a
479 statistically significant difference between the estimates obtained from the regression fits and those
480 obtained using AAPM Report 204 conversion factors. In addition, the SSDE-based estimates were shown
481 to be consistently lower by 32-50% than those provided by the regression fits of $D_{wt-avg,2}$ and $D_{wt-avg,3}$.

482 Thus, the conversion factors found in AAPM Report 204 do not appear to be applicable when the dose to
483 bone is included. Instead the dose to bone itself or the mass-weighted average dose may be used.

484 There are some limitations to this study. This study only investigated dose distributions from
485 voxelized phantom models and voxelized patient data from a single scanner model. In order to devise an
486 official SSDE for head CT examinations, the data presented in this study may be combined with other
487 physical air kerma measurements of head-sized phantoms and MC simulations from different scanner
488 models as was done for AAPM Report 204.⁵ Moreover, the voxelized phantom models used in this
489 investigation were of spatial low resolution. Despite the low resolution of the phantoms, dose distribution
490 within the brain parenchyma was still observed to be fairly uniform. This dose uniformity was observed
491 even for the voxelized patient models, which have much higher resolution. However, the low resolution
492 could affect the accuracy of surface bone dose (and mass-weighted average dose) due to volume
493 averaging used to make coarser voxels. Additionally, the patient table was not considered in these
494 simulation, the omission of which could lead to an overestimation of patient dose.²⁵ However, this
495 overestimation is expected to be under 10% relative to doses considering the inclusion of the table.

496 In summary, this study developed conversion coefficients for routine helical head CT procedures
497 using MC methods and voxelized patient models for two interpretations of “center of the scan volume”
498 that may be used in a manner similar to those described in in AAPM Report 204.⁵ In addition,
499 normalized dose coefficients were estimated as a function of patient size for both bone as well as a mass
500 weighted average of brain and bone, all in the middle of the scan volume. These may contribute to the
501 efforts to report size specific doses arising from CT exams.

502

503 **ACKNOWLEDGEMENTS**

504 This work was supported in part by a grant from the NIBIB (R01-EB017095) and by a grant from the
505 NIH (T32-EB002101). J.M.B is supported in part by NIH grants (R01-CA181081, R01-EB025829, and
506 R01-CA214515). A.M.H is supported in part by NIH grant R01-CA18108. C.H.M. receives research

507 support from Siemens Healthcare. M.M.G's department has a master research agreement with Siemens
508 Healthcare.

509

510

511 **REFERENCES**

512 ¹ R. Smith-Bindman *et al.*, "Radiation Doses in Consecutive CT Examinations from Five University
513 of California Medical Centers," *Radiology* **277**(1), 134–141 (2015).

514 ² C.H. McCollough, "CT dose: how to measure, how to reduce.," *Health Phys.* **95**(5), 508–17
515 (2008).

516 ³ M.F. McNitt-Gray, "AAPM/RSNA Physics Tutorial for Residents: Topics in CT Radiation Dose
517 in CT1," *Radiographics* **22**(6), 1541–1553 (2002).

518 ⁴ A.C. Turner *et al.*, "The feasibility of patient size-corrected, scanner-independent organ dose
519 estimates for abdominal CT exams.," *Med. Phys.* **38**(2), 820–9 (2011).

520 ⁵ AAPM Task Group 204, *Size-Specific Dose Estimates (SSDE) in Pediatric and Adult Body CT*
521 *Examinations* (College Park, MD, 2011).

522 ⁶ B.M. Moore, S.L. Brady, A.E. Mirro, and R.A. Kaufman, "Size-specific dose estimate (SSDE)
523 provides a simple method to calculate organ dose for pediatric CT examinations," *Med. Phys.*
524 **41**(7), 1–10 (2014).

525 ⁷ K. McMillan, M. Bostani, C. Cagnon, M. Zankl, A.R. Sepahdari, and M. McNitt-Gray, "Size-
526 specific, scanner-independent organ dose estimates in contiguous axial and helical head CT
527 examinations," *Med. Phys.* **41**(12), 121909 (2014).

528 ⁸ AAPM Task Group 220, *Use of Water Equivalent Diameter for Calculating Patient Size and Size-
529 Specific Dose Estimates (SSDE) in CT* (College Park, MD, 2014).

530 ⁹ N. Petoussi-Henss, M. Zankl, U. Fill, D. Regulla, and M. Zankl, "The GSF family of voxel
531 phantoms," *Phys. Med. Biol.* **47**(1), 89–106 (2002).

532 ¹⁰ International Commission on Radiological Protection, "Adult reference computational phantoms,"

533 ICRP Publ. 110. Ann. ICRP 39 (2), (2009).

534 ¹¹ M. Zankl, K.F. Eckerman, and W.E. Bolch, “Voxel-based models representing the male and
535 female ICRP reference adult - The skeleton,” Radiat. Prot. Dosimetry **127**(1–4), 174–186 (2007).

536 ¹² J.J. Demarco, T.D. Solberg, and J.B. Smathers, “A CT-based Monte Carlo simulation tool for
537 dosimetry planning and analysis,” Med. Phys. **25**, 1–11 (1998).

538 ¹³ American Association of Physicists in Medicine, *Adult Routine Head CT Protocols Version 2.0*,
539 1–20 (2016).

540 ¹⁴ D.B. Pelowitz, “MCNPX User’s Manual,” in *MCNPX User’s Man.*(Los Alamos, NM, 2011).

541 ¹⁵ AAPM Task Group 195, *Monte Carlo Reference Data Sets for Imaging Research* (College Park,
542 MD, 2015).

543 ¹⁶ M. Bostani *et al.*, “Accuracy of Monte Carlo simulations compared to in-vivo MDCT dosimetry.,”
544 Med. Phys. **42**(2), 1080 (2015).

545 ¹⁷ A.C. Turner *et al.*, “A method to generate equivalent energy spectra and filtration models based on
546 measurement for multidetector CT Monte Carlo dosimetry simulations.,” Med. Phys. **36**(6), 2154–
547 2164 (2009).

548 ¹⁸ ICRU, “ICRU Report 44, Tissue Substitutes in Radiation Dosimetry and Measurement,” J. Int.
549 Comm. Radiat. Units Meas. (1993).

550 ¹⁹ J.J. DeMarco *et al.*, “A Monte Carlo based method to estimate radiation dose from multidetector
551 CT (MDCT): cylindrical and anthropomorphic phantoms.,” Phys. Med. Biol. **50**(17), 3989–4004
552 (2005).

553 ²⁰ D. Zhang *et al.*, “Variability of surface and center position radiation dose in MDCT: Monte Carlo
554 simulations using CTDI and anthropomorphic phantoms.,” Med. Phys. **36**(3), 1025–38 (2009).

555 ²¹ ICRP 70, “Basic Anatomical & Physiological Data for use in Radiological Protection - The
556 Skeleton,” Ann. ICRP (2), (1995).

557 ²² M. Cristy, “Active bone marrow distribution as a function of age in humans.,” Phys. Med. Biol.
558 **26**, 389–400 (1981).

559 ²³ ICRP, “The 2007 Recommendations of the International Commission on Radiological Protection,”
560 ICRP Publ. 103. Ann. ICRP 37 (2007).

561 ²⁴ M.S. Pearce *et al.*, “Radiation exposure from CT scans in childhood and subsequent risk of
562 leukaemia and brain tumours: A retrospective cohort study,” *Lancet* **380**(9840), 499–505 (2012).

563 ²⁵ P. Nowik, R. Bujila, L. Kull, J. Andersson, and G. Poludniowski, “The dosimetric impact of
564 including the patient table in CT dose estimates,” *Phys. Med. Biol.* **62**(23), N538–N547 (2017).

565